



Strike-slip fault bridge fluid pumping mechanism: insights from field-based palaeostress analysis and numerical modelling

Michal Nemčok^{a,*}, Andreas Henk^b, Rodney A. Gayer^a, Sara Vandycke^{a,1}, Tanya M. Hathaway^{a,2}

^aLaboratory for Strain Analysis, Department of Earth Sciences, University of Wales, Cardiff CF1 3YE, UK

^bInstitute for Geology, University of Freiburg, Albertstrasse 23b, D-79104 Freiburg, Germany

Received 3 November 1999; received in revised form 10 December 2001; accepted 20 December 2001

Abstract

We present a finite-element study of stress perturbation in evolving compressive and extensional strike-slip fault bridges. The results are compared with a fracture study of a compressive bridge at St Donats, UK. Horizontally interbedded calcareous mudstone and bioclastic calcilitite at St Donats have a distinct vertical permeability anisotropy. This sedimentary sequence behaves as a set of horizontal aquifers. The fluid flow in these aquifers is sensitive to mean stress gradients. Paleostress analysis of field fracture data, verified by finite-element modelling, indicates a rotation of σ_1 towards parallelism with boundary faults inside the growing compressive bridge. Boundary faults and bridge faults recorded numerous fluid flow events. The modelled mean stress pattern shows a regional maximum within the bridge and local maxima/minima pairs at boundary fault tips.

Finite-element modelling of an extensional bridge indicates that σ_3 rotates towards parallelism with boundary faults. The mean stress pattern is similar to the pattern in compressive bridge but with maxima and minima locations interchanged. The stress patterns are reestablished by each stress build-up preceding the rapture of the boundary faults throughout the development stages of strike-slip fault bridges. Mean stress gradients developed pre-failure control the fluid flow in fractures of the strike-slip fault system at and after the end of each stress build-up and the fluid flow in boundary faults post-failure. Fracture reactivation and new fracture generation within an evolving bridge is a process consisting of multiple successive events that retain the storage capacity of the bridge. Rupture and sealing of the main bounding-faults is a step-wise process that opens and closes fluid conduits between areas with different pressures. © 2002 Elsevier Science Ltd. All rights reserved.

Keywords: Faults; Fluid flow; Strike-slip; Numerical modelling

1. Introduction

Controls exerted on fluid flow by active faults have been studied in a wide range of geologically related processes, ranging from hydrocarbon migration and hydrothermal ore deposition to seismicity (e.g. Parry and Bruhn, 1986, 1990; Forster and Evans, 1991; Byerlee, 1993; Sibson, 1994; Miller et al., 1996; Caine and Forster, 1999; Ferrill et al., 1999; Hardebeck and Hauksson, 1999; Tsang, 1999). One of the fault effects on fluid flow relates to the capability of active faults to perturb a regional stress field (e.g. Segall and Pollard, 1980; Gamond, 1987; Mandl, 1988; Jamison, 1996; Homberg et al., 1997; Ohlmacher and Aydin, 1997;

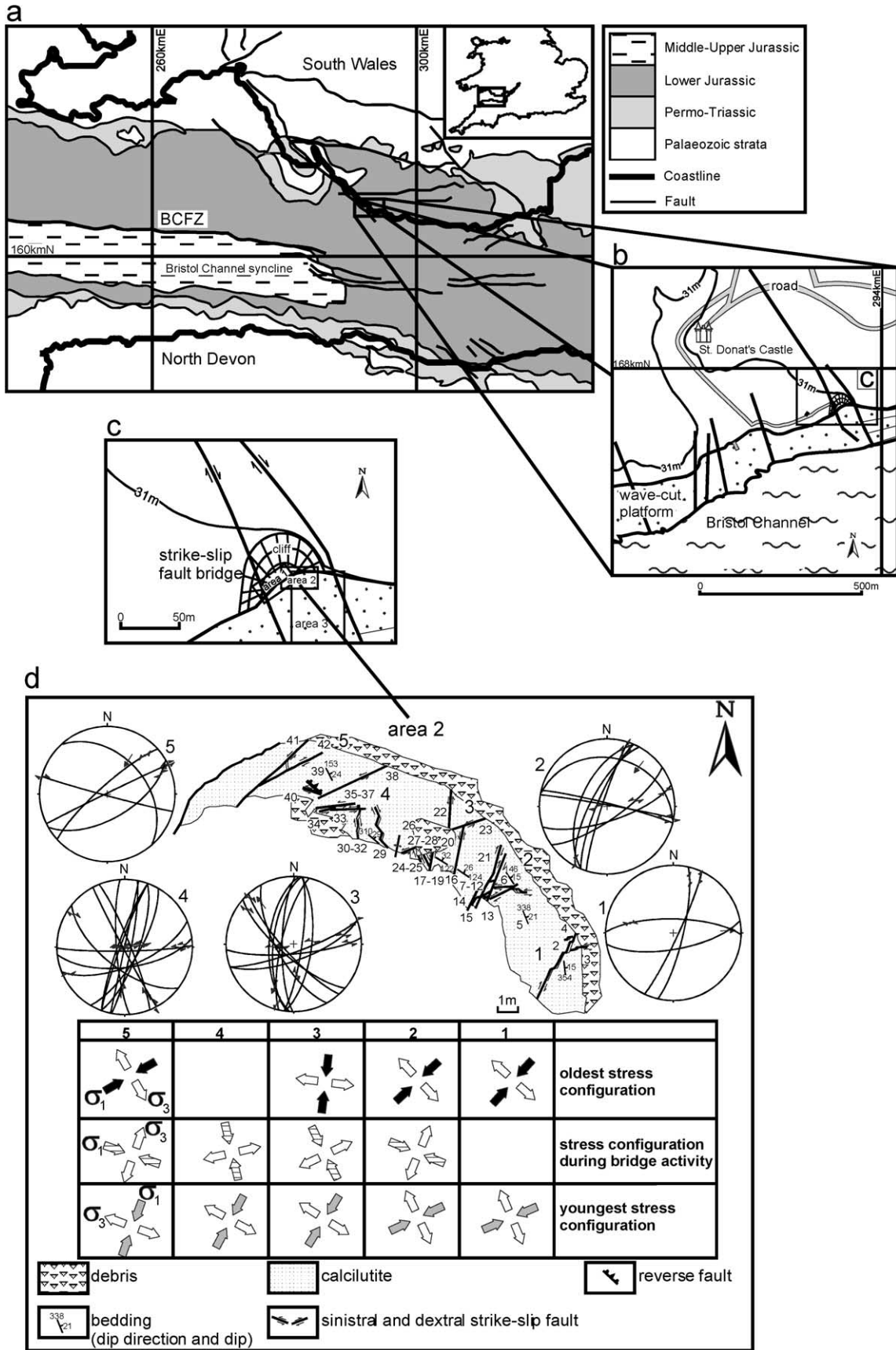
Martel and Boger, 1998). Each episode of the fault rapture and propagation, accompanied by elastic unloading, is triggered by preceding stress build-up (e.g. Yielding et al., 1981; Rockwell et al., 1988; Klinger and Rockwell, 1989; Philip et al., 1992; Treiman, 1995). Uniaxial and triaxial compression tests indicate that microfracturing begins as stresses build up to about half the fracture strength of the rock, and continue until the stress level reaches about 95% of fracture strength (Scholz, 1968). Similar relationships are valid for meso-scale fracture patterns associated with large faults (e.g. Martel et al., 1988; Willemse et al., 1997; Antonellini and Mollema, 2000). Fracturing/faulting relationships are very complex in evolving strike-slip bridges (Gamond, 1987; Ramsay and Huber, 1987), which have also been called relay ramps (Peacock and Sanderson, 1995), relays (Larsen, 1988) or stepovers (Aydin and Nur, 1985). The complexity is because (1) straining that utilizes a stress transfer (e.g. Geiser, 1974; Wojtal and Mitra, 1986; Mandl, 1988) penetrates into the strike-slip bridge from both sides, and (2) the shear softening record near each

* Corresponding author. Present address: Energy and Geoscience Institute, University of Utah, 423 Wakara Way, Salt Lake City, UT 84108, USA.

E-mail address: mnemcok@egi.utah.edu (M. Nemčok).

¹ Present address: Laboratoire de Géologie Fondamentale et Appliquée, Faculté Polytechnique de Mons, 9 rue de Houdain, 7000 Mons, Belgium.

² Present address: Robertson Research International Ltd, Llandudno, Gwynedd, North Wales, UK.



strike-slip fault rotates as the movement on the fault continues (e.g. Sylvester, 1988) and opposite rotations meet in the bridge.

The balance between fluid sources and diffusion in fractured rocks is complicated by cyclic changes in fracture permeability during stress build-up and release cycles (e.g. Carlsson and Olsson, 1979; Walsh, 1981; Oliver, 1986; Sibson, 1990; Knipe, 1993; Caine and Forster, 1999; Connolly and Cosgrove, 1999). The stages of a fault permeability cycle are: (1) fault zone permeability several orders of magnitude larger than host rock permeability; (2) progressively decreasing fault zone permeability; and (3) decrease of fault zone permeability to its residual stage (e.g. Nur and Booker, 1972; Booker, 1974; Walsh, 1981; Scholz, 1990; Knipe et al., 1991; Fisher et al., 1996; Roberts et al., 1996). Faults and fractures in the first stage capture a fluid flow, as documented by hydrologic (Moore et al., 1990) and geochemical studies (Davidson et al., 1998). Horizontally flowing fluids tend to be redistributed from areas of increased mean stress to areas of decreased mean stress (e.g. Nur and Booker, 1972). Fluids are driven out of compressive fault bridges where the mean stress increases in response to fault slip, while influx occurs in extensional bridges where mean stress is reduced (Sibson, 1985; Connolly and Cosgrove, 1999). The fluid regime before, during and after fault failure, documented by the artificial landslide experiments of Harp et al. (1990), shows fluid pressure increase during the pre-failure stage, fluid pressure drop due to dilatancy fracturing, major fluid pressure drop during failure and progressive fluid pressure dissipation post-failure.

The first goal of this paper is to present an analysis of fracturing in a field study of a compressive strike-slip bridge, in order to gain an insight into its behaviour during all three stages of the permeability cycle of the main bounding faults. The second goal is to present the results of a finite-element study concentrating on the principal stress and mean stress distributions, and failure criteria, during various stages of a strike-slip bridge development. This numeric study investigates compressive and extensional bridges in order to characterize both bridge types. The results of the study are discussed in terms of the likely effect of these bridges on the associated fluid systems, particularly as regards fluid sources and sinks.

2. Field study

2.1. Hydraulic characteristics of field example

Our study area consists of subhorizontally bedded Lower Jurassic rocks cropping out at St Donats (Fig. 1). The 150-m-thick section of shallow marine sediments is cut by early,

rifting-related WNW–ESE striking normal faults and extensional veins and a later, basin inversion-related NNW–SSE to N–S striking dextral strike-slip faults (Nemčok et al., 1995). Two of the latter, to the southeast of St Donats Castle, overlap and form between them a 65-m-wide and 280-m-long compressive bridge, which constitutes our study area. The St Donats area provides several features, described below, which increase the likelihood of the horizontal flow affected by mean stress distribution. The most important feature is the significantly different permeabilities of the interbedded, marine, grey calcareous mudstones and thin bioclastic calcilutites (Waters et al., 1987; Smith and Wiltshko, 1996) in which the bridge structures are developed. A distinct vertical permeability anisotropy in a subhorizontally-layered section is the major requirement for potential horizontal fluid flow (e.g. Magara, 1976; Bredehoeft et al., 1988; Mann and Mackenzie, 1990).

A detailed fracture study in these calcilutites and mudstones (Nemčok et al., 1995) showed that the aperture dimension along a single fracture varies over about one order of magnitude across the calcilutite/mudstone boundary (Fig. 2a). A simple analytical calculation for permeability in fractured media, following modified Navier–Stokes equation and Darcy's Law (e.g. Lee and Farmer, 1993) documents that a condition of distinct vertical permeability anisotropy holds also in the case when our intercalated calcilutite/mudstone section is fractured. Fracture permeabilities of the calcilutite and mudstone are three orders of magnitude different (Fig. 2b). Therefore, the section at St Donats retains a distinct vertical permeability anisotropy in the fractured state and calcilutites form subhorizontal aquifers.

As a consequence of the subhorizontal aquifer system in the sedimentary section, the elevation term, z , in the hydraulic head equation $h = z + p/\rho_t g$ (Hubbert, 1940) vanishes and the hydraulic head within each reservoir layer is controlled by fluid pressure gradients. Fluid pressures and fracture permeabilities are coupled with mean stress gradients (e.g. Walsh, 1981; Oliver, 1986; Sibson, 1990; Connolly and Cosgrove, 1999). Therefore, the determination of the mean stress distribution in the St Donats outcrop allows a prediction that the fluid flow trends follow the mean stress gradients.

2.2. Field observations at St Donats

Fracture mechanisms in the study area were determined using the kinematic indicators described by Hancock (1985) and Petit (1987). Areas 1–3 in Fig. 1c were mapped using photographs and area 3 was divided into a rectangular, 1.5 m by 2 m grid prior to photography.

Fig. 1. (a) Geological map of the inner Bristol Channel, located in the insert map of the southern British Isles. (b) Map of the St Donats Castle area, showing the boundary faults of the strike-slip fault bridge. (c) Detail of part of the fault bridge studied, located in (b), and showing the three areas described in the text. (d) Geological map of area 2 located in (c) showing the computed σ_1 and σ_3 stresses of the oldest and youngest stress configurations and configuration active during the compressive bridge development. Meso-scale fault-striae data from the five sub-areas are plotted in lower hemisphere stereographic projections. Data tables are available in the JSG electronic annex.

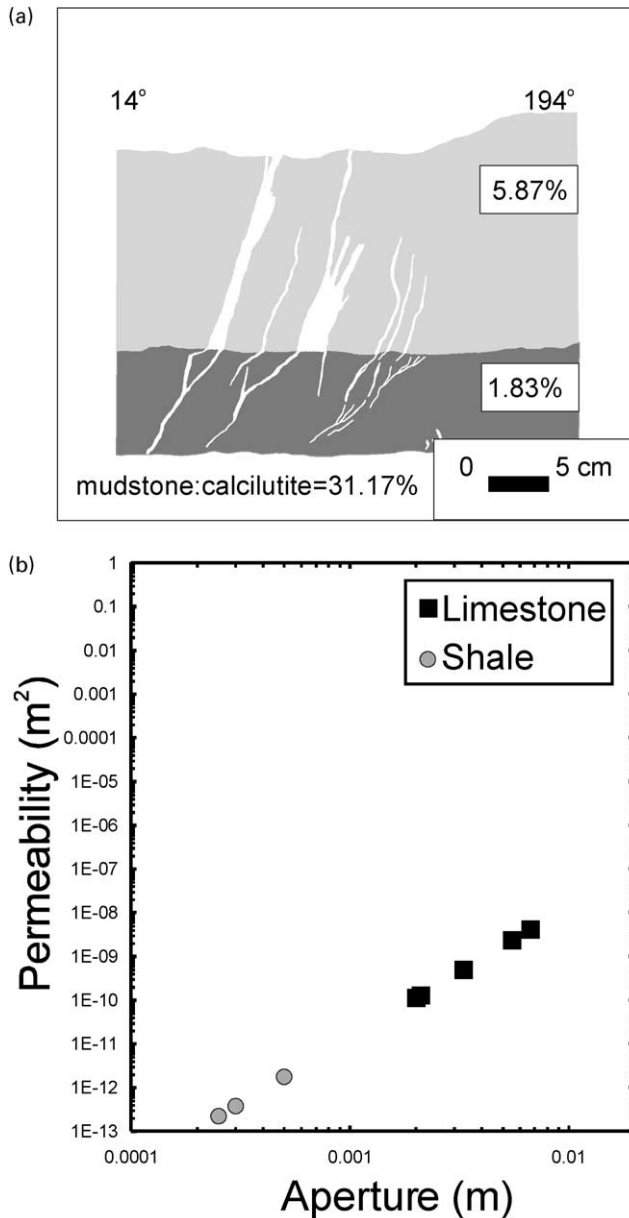


Fig. 2. (a) Fracture aperture dependence on rock rheology indicated by fracture porosity modified from Nemčok et al. (1995). Light pattern indicates bioclastic calcilutite and dark pattern indicates calcareous mudstone. Fracture porosity for each layer and fracture porosity ratios are expressed as percentages. (b) Variation in permeability, expressed as the coefficient of hydraulic conductivity, with fracture aperture, related to fractures which propagate from mudstone to calcilutite. Calculation, following Darcy's Law and Navier–Stokes equation modified by Snow (e.g. Lee and Farmer, 1993), assumes a fluid density, ρ_f , of 1000 kg m^{-3} , a dynamic fluid viscosity, η , of $1 \times 10^{-3} \text{ kg m}^{-1} \text{ s}^{-1}$ (Freeze and Cherry, 1979) a hydraulic gradient ratio, I , of 0.06 (Caine, 1999) and a fracture width of 0.173 m. Equations are: $Q = -a^3 \rho_f g / 12 \eta / W$ and $k = \eta Q / \rho_f g I A$, where k is the coefficient of hydraulic conductivity, Q is the volumetric flow rate in direction of decreasing pressure, A is cross-sectional area across which the perpendicular discharge Q flows, g is the gravity acceleration, a is the fracture aperture, and W is the fracture width.

The area studied at St Donats is deformed by two overstepping dextral strike-slip faults, exposed on the wave-cut platform and in the cliff section (Fig. 1). They have a parallel strike of 337° and are called the boundary faults. Transient fluid flow along the west boundary fault is documented by the presence of multiple calcite crusts along the fault plane, each with differently oriented striations, each precipitated during a different slip event (Fig. 3a). The compressive bridge between the boundary faults is internally deformed mostly by meso-scale faults, along which dilatational jogs, filled with calcite cements are separated by uncemented portions (Fig. 3b), resulting in a heterogeneous permeability structure. They are called bridge faults. Tips of bridge faults are formed by multiple generations of solution seams, pull-aparts and en échelon veins, which document a series of multiple failure and fluid events (Fig. 3c). There are two sets of calcite veins inside the bridge. The older set, coeval with normal faults of the same WNW–ESE strike, is developed both outside and inside the bridge and is cross-cut by all the fractures developed inside the bridge (Fig. 4). The younger set of veins, related to the internal deformation of the compressive bridge, is developed only along the boundary faults. Bridge faults in areas 1, 2 and 3 in Fig. 1c are mostly either dextral or sinistral strike-slip faults, but also, less commonly, oblique-slip faults with a reverse or normal component of displacement. Calcite precipitated in pressure shadows allows a simple and unambiguous determination of their displacement sense. Area 2 in Fig. 1c, located at the compressive bridge centre, is deformed also by stylolites, whose normals plunge sub-horizontally towards WSW. No larger veins are present in this area, only pull-aparts along bridge faults. The cross-cutting relationships of various bridge faults suggest the activity of either two or three tectonic events. Area 3 in Fig. 1c, located near the eastern boundary fault, contains bridge faults of various strikes cross-cutting a WNW–ESE striking pattern of veins and normal faults, formed prior to the bridge development (Fig. 4). Bridge faults include dextral R shears, varying in strike from N–S to NNE–SSW, and P shears varying in strike from NW–SE to NNW–SSE. Both R and P shears are cut by several generations of R' shears, ranging in strike from E–W to NE–SW.

2.3. Stress and strain data at St Donats

In order to calculate paleostresses from field fracture data, we used the method of Hardcastle and Hills (1991) for four or more faults (Table 1). P and T stress axes and principal strain axes, following Hardcastle (1989), were calculated from smaller fault populations. Results of this calculation are available in the JSG electronic annex. The computational separation of faults into sets related to older and younger stress states matches the field separation of the bridge faults into relatively older and younger, based on cross-cutting relationships. The cross-cutting relationships

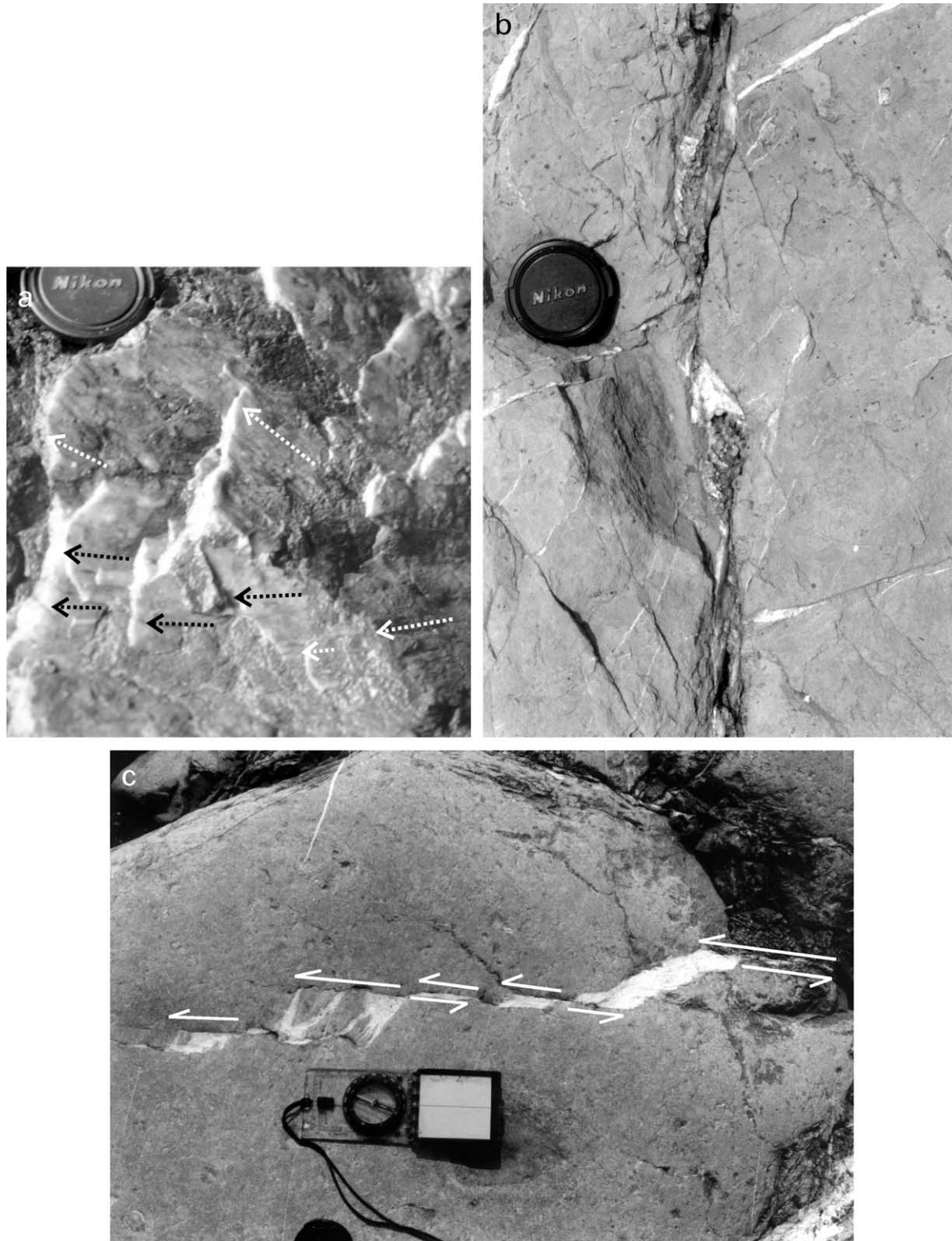


Fig. 3. (a) Photo of the west boundary fault of the St Donats compressive bridge. Average fault strike from the geological map in Fig. 1b is 337° and local strike and dip of this part of the fault plane is 305 and 86° to the west, respectively. Fault plane is lined by calcite precipitated in multiple layers. Each layer relates to a different rupture and fluid flow event and records a specific displacement vector. Arrows indicate movement of the missing block. (b) Photo of a sinistral R' shear from area 3 of Fig. 1c. Permeability structure and friction of this fault is heterogeneous, because calcite cement is concentrated only within dilatational jogs. Portions of this fault that have not experienced extensive dilation remained uncemented. (c) Photo of a sinistral R' shear tip from area 3 of Fig. 1c, recording multiple episodes of propagation facilitated by generations of solution seams, pull-aparts, en échelon veins and shear fractures.

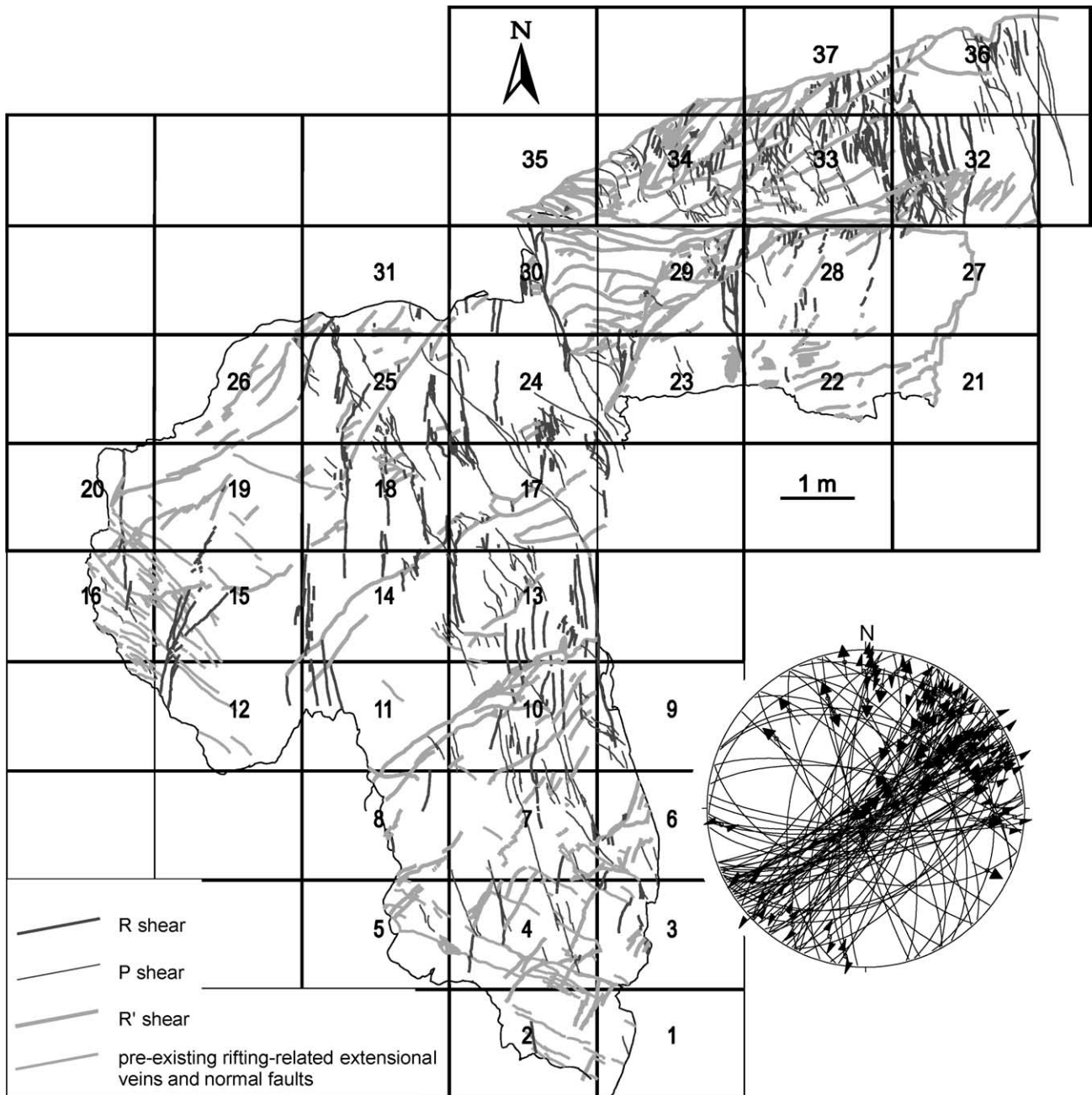


Fig. 4. Structural map of area 3 located in Fig. 1c showing numbered rectangles of the mapped grid with faults and veins. Data are available in the JSG electronic annex. Rectangles 28–37 show several cross-cutting generations of sinistral R' shears. E–W shears are cross-cut by NE–SW shears (e.g. boundary of rectangles 28 and 33) and they in turn are cross-cut by NNE–SSW shears (e.g. boundary of rectangles 23 and 29).

of various bridge faults suggest the activity of either two (sub-areas 1 and 4 in Fig. 1d) or three (sub-areas 2, 3 and 5 in Fig. 1d) different stress fields. The oldest and youngest stress fields are characterized by a NE–SW oriented σ_1 and a NW–SE σ_3 . The intermediate stress field has NW–SE oriented σ_1 and NE–SW oriented σ_3 . The oldest and youngest stress fields (Fig. 1d) have also been identified from damage zones of boundary faults and fault data outside the bridge (see also Nemčok et al., 1995), in which there is no indication of the existence of an intermediate stress

regime (Fig. 1d). Therefore, it is concluded that the intermediate stress field is coeval with the bridge development. The σ_1 stress orientation of the intermediate stress regime is parallel to the stylolitic normals measured in area 2 in Fig. 1c, located at the compressive bridge center. Although three stress regimes have been calculated from the fracture data of area 3 as a whole, none of the grid rectangles shows the complete relative sequence of related deformational events. Rectangles 1, 2, 4, 8, 10, 12, 13, 16, 17, 20, 24, 30, 32 and 34 (Fig. 4) show the relationship between the youngest and

Table 1
Principal stress orientations calculated from the faults in area 1 (a) and 3 (b) in Fig. 1c. The reading of each stress axis includes trend/plunge. The stress ratio R equals $(\sigma_2 - \sigma_3)/(\sigma_1 - \sigma_3)$

(a)					
Event	Zone	σ_1	σ_2	σ_3	$(\sigma_2 - \sigma_3)/(\sigma_1 - \sigma_3)$
Older	1	068/25	184/44	318/36	0.1
Older	2	036/20	259/64	132/17	0.1
Older	2	056/30	236/60	326/00	0.1
Younger	1	026/25	243/60	124/16	0.1
Younger	2	011/20	198/70	101/02	0.1
Younger	3	032/30	197/59	298/07	0.5
(b)					
Event	Rect.	σ_1	σ_2	σ_3	$(\sigma_2 - \sigma_3)/(\sigma_1 - \sigma_3)$
Older	32	231/40	029/48	132/12	0.5
Younger	32	191/30	011/60	281/00	0.1
Younger	37	211/40	358/45	106/17	0.5

intermediate events. Rectangles 2, 28–30, 32, 34 and 37 show the relationship between the youngest and oldest events. Rectangles 10, 18 and 33 show the relationship between the intermediate and oldest events. Rectangles 34 and 37 are the only sites in the whole bridge where some cross-cutting relationships are contradictory; in these rectangles we have used the majority criterion for cross-cutting relationships (66.6%). We interpret these anomalous relationships to indicate finer stress fluctuations, beyond the resolution of the palaeostress analysis.

3. Numerical modeling of the stress within a bridge

3.1. Finite-element model specifications

In order to gain a quantitative understanding of the mean stress, principal stresses and differential stress versus rock

failure criteria in strike-slip fault bridges, we have carried out a number of finite-element models. Although the geometry of some models resembles the 65-m-wide and 280-m-long compressive bridge with dextral boundary faults at St Donats (Fig. 1b), modelling results have general implications, because we have studied four different boundary fault overlaps, representing successive stages of the bridge development, two boundary fault frictions and three stress ratios for both compressive and extensional bridges systematically (Table 2).

Each numerical model describes a three-dimensional block of rock with isotropic and homogeneous elastic properties, which is broken by two vertical planes of weakness, i.e. pre-existing boundary faults (Fig. 5). Normal stresses and strains are related by the generalized Hooke's law, available in any textbook (e.g. Mandl, 1988). As linear elasticity is a simplified description of the real rock rheology, we do not attempt to predict absolute values but concentrate on the relative patterns of deformation and stress in relation to different parameters (Table 2).

The models do not provide a direct indication of the evolution of stress in strike-slip fault bridges as their boundary faults propagate and the bridge configuration changes, because the models are unable to incorporate the propagation of the faults themselves. No assumptions are made about potential residual stresses in the bridge associated with its earlier stress history, when the amount of boundary fault overlap was less.

Pre-existing boundary faults in the numerical model are described by contact elements, transmitting stress. Transmitted tangential force, F_s , cannot exceed $|F_s| \leq -\mu F_n$, where F_n is the normal force and μ is the friction coefficient of the boundary fault. The contact stiffnesses with values close to elastic moduli of wall rocks are used to enforce compatibility between fault surfaces.

Modelling is made using the program ANSYS® (Ansys Inc., Houston, USA). 1680 eight-node isotropic brick elements are used to describe a model of 825 m length,

Table 2
Geometries and stress states of finite-element models A1 to H3. Models C41–C43 and G41–G43 have no cohesion and fault friction of 0.4. Remaining models have fault friction of 0.2. While the value of 0.4 describes mineralised faults (e.g. Hardcastle, 1989), the value of 0.2 honours the observation that calcite is present only in dilational portions of faults (Fig. 3b). The ratio of stress magnitudes, R , is defined as $(\sigma_2 - \sigma_3)/(\sigma_1 - \sigma_3)$. Stress magnitudes were calculated from paleostress data, shear failure criterion and amount of overburden. The calculation method is discussed in detail by Angelier (1989), and shear failure criterion and overburden by Nemčok and Gayer (1996)

Bridge	Relationship of bounding strike-slip faults	Stress magnitude ratio 0.1	Stress magnitude ratio 0.4	Stress magnitude ratio 0.8
		$\sigma_1 = 92.8$ MPa $\sigma_2 = 27.8$ MPa $\sigma_3 = 20$ MPa	$\sigma_1 = 38.2$ MPa $\sigma_2 = 27.8$ MPa $\sigma_3 = 20$ MPa	$\sigma_1 = 29.1$ MPa $\sigma_2 = 27.8$ MPa $\sigma_3 = 20$ MPa
Extensional	100 m underlap	A1	A2	A3
	0 m overlap	B1	B2	B3
	100 m overlap	C1, C41	C2, C42	C3, C43
	200 m overlap	D1	D2	D3
Compressive	100 m underlap	E1	E2	E3
	0 m overlap	F1	F2	F3
	100 m overlap	G1, G41	G2, G42	G3, G43
	200 m overlap	H1	H2	H3

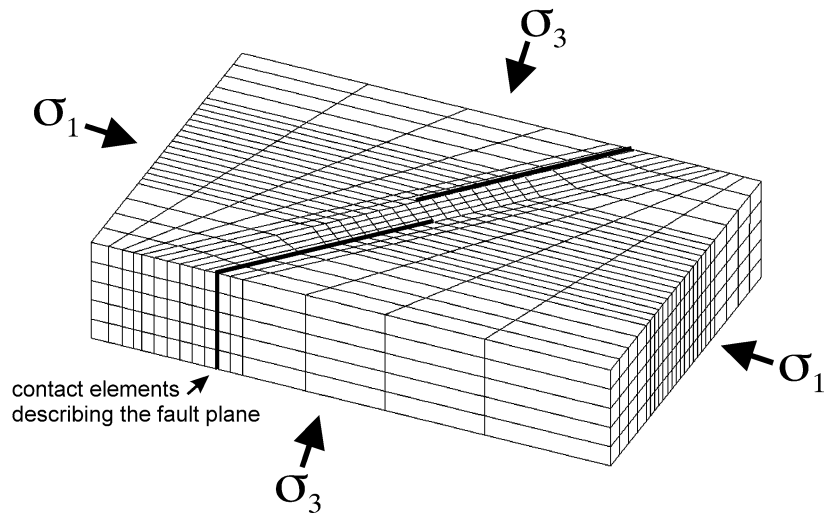


Fig. 5. Block used for finite-element modelling; 825 m long, 650 m wide and 200 m thick, divided into 1680 eight-node isotropic brick elements. The dimensions are sufficient to prevent edge effects in the model centre, where stresses between boundary faults of the bridge are investigated.

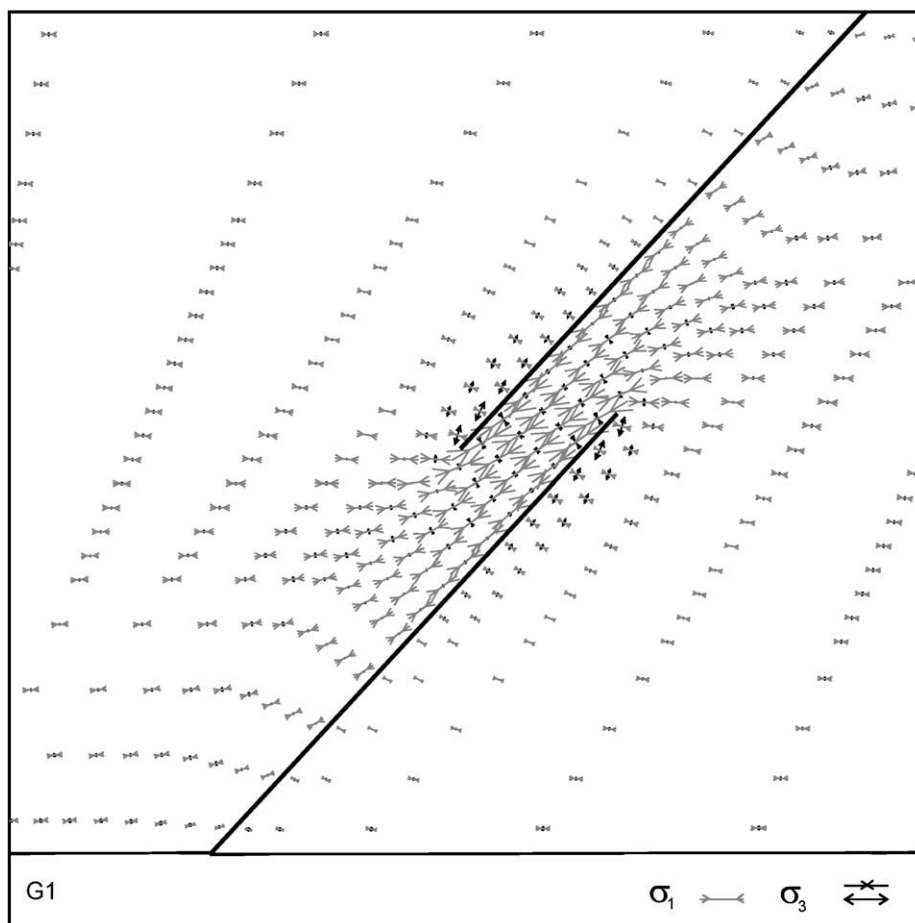


Fig. 6. Vector plot of the principal stresses for the G1 model of the compressive strike-slip fault bridge from Table 2, which is the mature bridge development stage. Figure shows only principal stresses located at 80 m below the surface of the modelled block (outcrop level at St Donats). Model indicates a significant stress perturbation characterised by counterclockwise σ_1 stress rotation inside the bridge, as high as 43° . This counterclockwise σ_1 stress rotation is in accordance with the σ_1 stress orientation calculated from bridge faults shown in Fig. 1d. Applied stresses and fault friction are listed in Table 2. Our models indicate that mature compressive bridges experience larger stress perturbation than less mature ones.



Fig. 7. Mean stress contour plots for selected G models of the compressive strike-slip fault bridge. Development stages of the bridge, fault friction and applied stresses are listed in Table 2. Mean stress values are normalised with respect to far-field values by division, where far-field values of the mean stress are 46.87, 28.67 and 25.63 MPa for stress magnitude ratio $R = 0.1, 0.4$ and 0.8 , respectively. Contour interval is 0.5.

650 m width and 200 m thickness (Fig. 5). The dimensions are such that edge effects are negligible in the centre of the model, which is investigated. Lithostatic pressure and no vertical displacements are used as boundary conditions for the upper and lower surfaces of the model, while tectonic stresses are applied as boundary conditions on the vertical sides of the model. The mechanical properties used for argillaceous calcilutites include a Young's modulus of 60 GPa taken from rock mechanics tables (Lama and Vutukuri, 1978) and a Poisson ratio of 0.344 determined from the nearby outcrop (Davies et al., 1991).

3.2. Models of principal stresses in compressive bridge

The results of the finite-element modelling show that the maximum principal compressive stress σ_1 progressively

rotates towards parallelism with the boundary faults as the compressive bridge develops by progressive propagation of the boundary-fault tips, forming the bridge inside the 100 m underlap, 0 m overlap, 100 m overlap (Fig. 6) and 200 m overlap. Calculated orientations of principal stresses are in accordance with those calculated from bridge fault data coeval with bridge activity (Fig. 1d). Scaled principal stress vectors in Fig. 6 indicate that the most dramatic stress perturbation occurs in the tip regions of both boundary faults. Fault slip in the advancing side or compressional quadrant of the boundary fault tip magnifies σ_1 stress and the retreating side or extensional quadrant magnifies σ_3 stress.

Compatibility of the numeric results with stresses determined from the observed bridge fractures and deformation sequence at St Donats allows us to proceed to mean stress modelling, assuming that the results would provide a

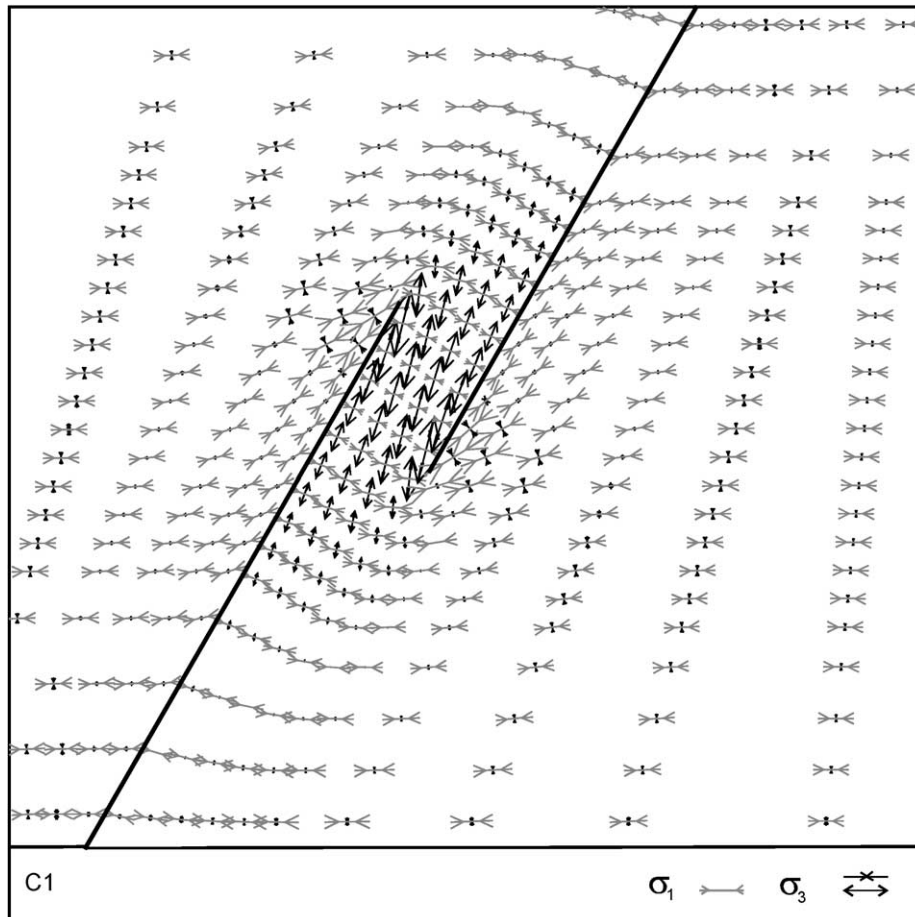


Fig. 8. Vector plot of the principal stresses for the C1 model of the extensional bridge from Table 2, which is the mature bridge development stage. Figure shows only principal stresses located at 80 m below the surface of the modelled block (outcrop level at St Donats). Model indicates a significant stress perturbation characterised by clockwise σ_1 stress rotation inside the bridge, as high as 31° . Applied stresses and fault friction are listed in Table 2. Our models indicate that mature extensional bridges experience larger stress perturbation than less mature ones.

reasonable analog to the mean stress that existed in the St Donats compressive bridge. Based on this encouragement, the parametric numeric modelling is expanded to cover also stress perturbations in extensional bridges.

3.3. Models of mean stress in compressive bridges

The results show the capability of boundary faults in the compressive bridge area to increase the mean stress during all simulated stages of the bridge development. The mean stress pattern can be characterized as having a regional maximum, located in the bridge centre and two local maxima/minima couples, formed in the boundary fault tip regions. The local maximum stress region is developed at the advancing side or compressional quadrant of the boundary fault tip. The local minimum is developed at the retreating side or extensional quadrant of the boundary fault tip. Models (Fig. 7) show that stress states with the lowest stress ratio R (Table 1) develop the most pronounced mean stress maxima/minima in the boundary fault tip regions. This is valid for each bridge development stage. The characteristic feature of a compressive bridge is that the relative motions

of the advancing sides of the two propagating boundary faults are opposed in the bridge. It is the stress build-up of these advancing sides that controls the mean stress concentration. The mean stress history in the regional minimum is more-or-less similar to the mean stress history in the tip regions. In all bridge development stages the stress states with higher σ_1 (Table 1) develop higher mean stress concentration. The mean stress at the regional maximum increases for all three stress ratios (Table 1, Fig. 7) when the boundary fault configurations vary from the 100 m underlap stage, through zero overlap to the 100 m overlap stage. The mean stress then remains more-or-less constant as the overlap increases to the 200 m overlap configuration, with only the size of the affected region increasing. Fig. 7 also shows that reduced friction along boundary faults enhances the mean stress increase inside the bridge.

3.4. Stress models of extensional bridges

In many ways the stress development in an evolving extensional bridge mirrors that of a compressive bridge described above. The modelled minimum principal compressive



Fig. 9. Mean stress contour plots for selected C models of the extensional strike-slip fault bridge. Development stages of the bridge, fault friction and applied stresses are listed in Table 2. Mean stress values are normalised with respect to far field values as in Fig. 7. Contour interval is 0.5. Negative values are calculated in cases where σ_3 , and sometimes σ_2 , stress inside the bridge is negative.

stress σ_3 progressively rotates towards parallelism with the boundary faults as the geometry of the extensional bridge develops from the 100 m underlap to the 200 m overlap (Fig. 8) stage. The model results indicate the capability of the boundary faults in the extensional bridge area to decrease the mean stress during all simulated stages of its development (Fig. 9). The mean stress pattern is characterized by a regional minimum, localized inside the bridge, and two local maxima/minima couples, formed at the advancing/retreating sides, respectively, in the tip regions of the boundary faults. Models (Fig. 9) show that stress states with the lowest stress ratio R (Table 1) develop the most pronounced mean stress maxima/minima in the boundary fault tip regions. This is valid for each bridge development stage. The characteristic feature of an extensional bridge is that the retreating sides of the two propagating boundary faults meet in the bridge. It is the interaction of these retreating sides that controls the mean stress decrease. In all bridge development stages, stress states with higher σ_1

(Table 1) develop a less intense mean stress decrease. Models show how the mean stress decrease in the bridge centre becomes larger for all three tested stress ratios when the boundary faults configurations vary from the 100 m underlap stage through zero overlap to the 100 m overlap stage. The mean stress then remains more-or-less constant as the configuration of the boundary faults changes towards the 200 m overlap stage, but the size of the affected region increases. Fig. 9 also shows that reduced friction along boundary faults enhances the mean stress decrease inside the bridge.

4. Discussion

4.1. Potential fluid flow characteristics predicted from the modelled mean stress distribution

It has been described earlier that the St Donats sedimentary

section comprises a set of subhorizontal aquifers. This section and similar subhorizontally layered sections with pronounced vertical permeability anisotropy are prone to have hydraulic head gradients controlled by the pressure term and to horizontal flow, as known, for example, from the Caspian Basin (Bredehoeft et al., 1988). The pressure term is controlled by the mean stress σ_m and pore fluid pressure p related through the porosity change $-\partial n$ of the fractured host rock and its compressibility α_n ($\alpha_n = -\partial n / \partial(\sigma_m - p)$) (Shi and Wang, 1986). In this special case, knowledge of the mean stress distribution provides an insight into the fluid flow directivity. The results of finite-element modelling (Figs. 7 and 9) indicate that the greatest mean stress gradients occur at the boundary fault tips. This determination is in accordance with 2D models of Segall and Pollard (1980). The local mean stress maximum at the advancing side of the boundary fault tip coupled with the local mean stress minimum at the retreating side of the tip drive the fluid flow around the fault tip, where the stress maximum forms the fluid source and the stress minimum forms the fluid sink. Also important fluid driving forces are the regional mean stress maxima and minima in compressive and extensional bridges, respectively, because of their areal extent. The mean stress concentration inside a compressive bridge drives fluids out of the bridge, whereas the mean stress decrease inside an extensional bridge drives fluids into the bridge. Models (Figs. 7 and 9) indicate that the average mean stress anomaly within the bridge differs by half an order of magnitude from the far field mean stress value. Models also indicate that the build-up of these mean stress anomalies develop during each pre-failure stage of the stress build-up and occur during the whole bridge development, thus providing a long-lasting fluid driving mechanism.

4.2. Assumed permeability gradients

Given a sufficient source of fluid, the fluid flow paths include bulk flow through the competing sediments' matrix and fracture networks, providing permeability gradients in the rock section (e.g. Knipe et al., 1991; Knipe, 1993). The modelled mean stress patterns (Figs. 7 and 9) progressively develop during the stress build-up that precedes each rupture event along boundary faults as their tips continue to propagate towards an increased overlap in the bridge area. Each stress loading stage close to boundary fault rupture and tip propagation is characterized by microfracturing that develops at stresses between 50 and 95% of fracture strength of the rock (Scholz, 1968). These fractures are known to act as small fluid reservoirs prior to the main faulting event Knipe et al. (1991). At higher stresses, the microfracture development accelerates and clusters until a shear fracture propagates through the rock (Krantz and Scholz, 1977) and microfracturing is confined to a damage zone around the propagating fracture (Lockner et al., 1992). The failure stage at the end of each stress build-up cycle triggers a

displacement of the boundary fault, which connects various strike-slip bridges and jogs, each characterized by its own fluid pressure anomaly. The open fractures along the boundary fault create a major migration pathway until either they undergo the aperture reduction toward a residual value when fluid pressure is decreased by fluid discharge or the fault zone is sealed by mineral precipitation (e.g. Harp et al., 1990; Moore et al., 1990; Sreaton et al., 1990; Davidson et al., 1998; Caine and Forster, 1999). Such cyclic variation of fracture permeability structure has been described by numerous workers (e.g. Carlsson and Olsson, 1979; Walsh, 1981; Oliver, 1986; Sibson, 1990; Knipe, 1993; Caine and Forster, 1999; Connolly and Cosgrove, 1999) and natural occurrences of fluid flow along major strike-slip fault systems have been cited by Jiang et al. (1997), Connolly and Cosgrove (1999) and Ferrill et al. (1999).

The flow rate along the boundary fault, understood as a fault core surrounded by damage zone (Chester and Logan, 1986; Smith et al., 1990), immediately after rupture is influenced by fluid pressure differential across the fault segment (Last and Harper, 1990). In our case fluid pressure anomalies in the bridges localised along this boundary fault, coupled with mean stress anomalies, contribute to this differential. As shown by the cubic law of flow in fractures (e.g. Last and Harper, 1990; Jiang et al., 1997), $Q = -k_f a^3 \Delta p / l$, the flow rate Q depends on the cube of the fault aperture a , the permeability factor k_f , the developed fluid pressure gradient Δp across a fault segment between neighbour bridges and the distance l along the boundary fault between bridges. The closer the proximity of the compressive and extensional bridges along the main fault, the larger will be the post-failure flow rate along the boundary fault. Increased fault aperture, permeability and gradient between fluid pressure anomalies, affected by mechanical stresses applied to the system across the fault segment and in bridges, also increase the flow rate. It should be stressed that the fault descriptors a , k_f and l simulate the behaviour of the fault zone, which is a complex fracture system in nature (e.g. Caine and Forster, 1999, and references therein).

The boundary fault slip type determines whether bridges with different fluid pressures become rapidly linked and develop fluid flow between them with or without the character of seismic pumping (e.g. Scholz, 1990; Sibson, 1994).

The ability of the bridge to store and transmit fluid is dependent on the orientation of the fracture pattern within the bridge in relation to the principal stress orientations, which control fracture apertures (e.g. Barton et al., 1995; Finkbeiner et al., 1997; Jiang et al., 1997; Ferrill et al., 1999). Fluid pressure affects the failure and slip, and in turn the mechanical stresses affect fluid pressure and fracture conductivity (e.g. Last and Harper, 1990).

4.3. Comparison among permeability gradients, modelling results and St Donats field data

The types of bridge fractures depend on the failure

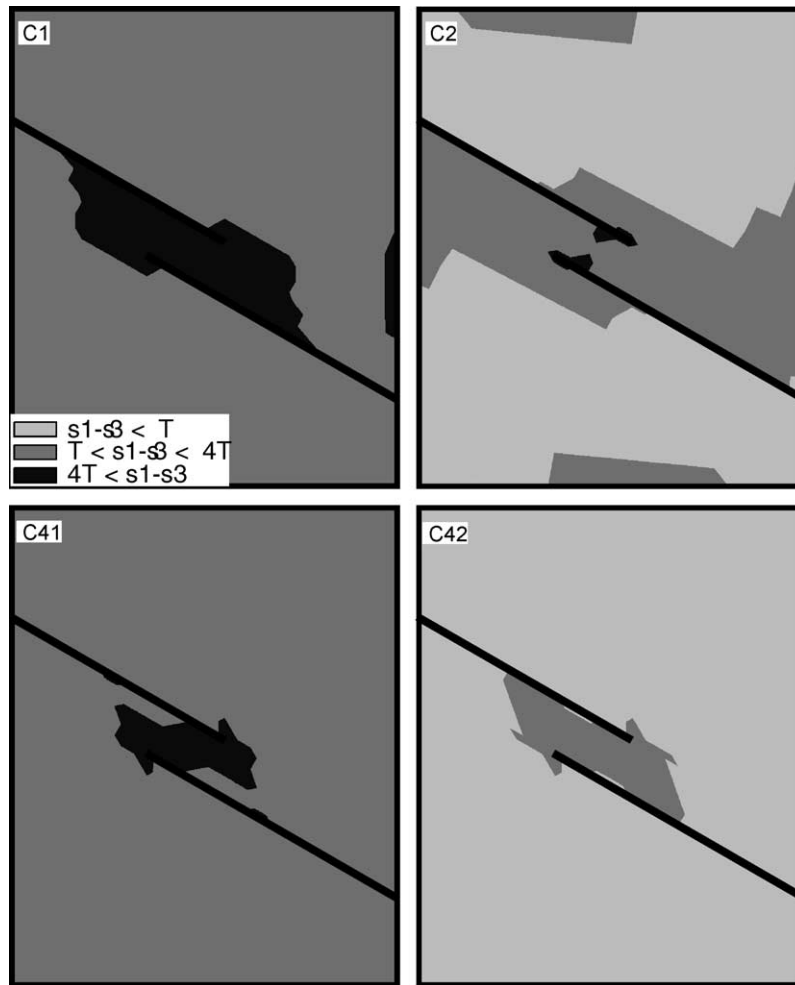


Fig. 10. Plots comparing differential stress $\sigma_1 - \sigma_3$ with tensile strength, T , of the calcitite host rock in order to determine areas of potential for hydraulic extension fractures ($\sigma_1 - \sigma_3 < 4T$) and extensional shear fractures (Griffith criterion, $4T < (\sigma_1 - \sigma_3) < 6T$) in compressive bridges. Stress state with stress magnitude ratio R of 0.1 is capable of triggering the extensional fracturing inside the compressive bridge during all its development stages. This capability is enhanced by increased friction along boundary faults. Stress states with less prominent σ_1 have a capability of triggering extensional fracturing better in more mature stages of the bridge development. Fracturing by shear fractures or faults inside the bridge, which was observed in the field, requires increased fluid pressure to meet the failure condition.

criteria and conditions achieved by stress build-ups during the whole bridge development history. Extensional fractures at St Donats are developed only along the boundaries of the compressive bridge. The main portion of the compressive bridge is deformed by shear fractures. However, our modelling of the failure conditions (Fig. 10) does not show a sufficiently high differential stress for the development of shear fractures inside the bridge. Shear fractures inside the bridge, thus, indicate that fluid pressure was significant, shifting the Mohr stress circle towards the failure envelope. An independent indication of fluid flow events inside the bridge is the presence at the bridge fault tips of multiple generations of en échelon veins and pull-aparts filled by calcite (Fig. 3c). Evidence of transient fluid flow along the boundary fault is the multiple calcite generations related to different slip events (Fig. 3a).

The factor influencing the storage capacity of the bridge faults is the cyclic sequence of reactivation, comprising

periods of rupturing followed by cementation with calcite. Both mechanisms are geologically fast. Rupturing lasts from several seconds to tens of seconds (e.g. Sibson, 1989). Mineral precipitation lasts from hours to months (e.g. Grindley and Browne, 1976; Batzle and Simmons, 1977; Kukal, 1989).

4.4. Comparison of modelled mean stress with St Donats field data

The modelled mean stress increases inside the compressive bridge during multiple stress build-ups during the whole bridge development history (Fig. 7). The increase is a consequence of the opposed relative motions of the two propagating bridge boundary faults. These advancing fault sides have been also described as compressional quadrants, and are identified by the presence of stylolites, compaction bands or other strain softening features in various lithologies

(e.g. Gamond, 1987; Mollema and Antonellini, 1996; Willense et al., 1997). In the bridge the stress transfer utilised by straining from two sides meets. The observed bridge faults indicate that the bridge deformation includes also a rotational component. Several generations of sinistral R' shears in rectangles 29–37 of area 3 (Fig. 4) inside the compressive bridge, indicate this rotation, the precise amount of which is difficult to determine because the perturbed stress inside the bridge during its development also affects the orientation of the bridge faults. Therefore, a comparison of ideal orientations of P, R and R' faults of 318, 356 and 29°, respectively, with measured ranges of 317–343° for P, 350–24° for R and 23–96° for R' faults provides only an indication of the combined rotational component of deformation and stress perturbation inside the compressional bridge. The comparison between the ideal and measured orientations of bridge faults, combined with the cross-cutting relationships of bridge faults (Fig. 4) implies that the lower limit of the range of strike values for each fault type is the youngest generation of faults and that they developed in ideal orientations.

The increased stress perturbation during the bridge development, indicated in Fig. 6, together with recognised rotation of earlier bridge faults to slightly different positions implies that bridge faults undergo aperture changes during the bridge development history.

5. Conclusions

1. The Lower Jurassic sedimentary section at St Donats has over three orders of magnitude permeability difference between interbedded bioclastic calcilutite and calcareous mudstone even after fracturing. This section, with laterally continuous seals and aquifers, meets the requirements for large-scale lateral fluid flow.
2. The elevation term in the horizontal reservoir layers vanishes and the hydraulic head is controlled by fluid pressure gradients, which are affected by mechanical stresses and in turn affect the failure and slip. It is therefore possible to use the modelled mean stress to predict the fluid flow trends.
3. Palaeostress analysis of fractures developed in the compressive bridge at St Donats indicates the existence of at least three successive stress states. The early and late stress patterns were parallel to the regional stress field. The intermediate stress pattern, coeval with the bridge development, indicates a rotation of the maximum principal compressive stress σ_1 towards parallelism with boundary fault strikes during progressive fault overlap and growth of the compressive bridge area.
4. Extensional fractures in the St Donats compressive bridge were developed only at its boundaries. The internal portion of the bridge is deformed almost exclusively by shear fractures, although stylolites are also present in a small central area. Numeric modelling, however, indicates that failure conditions for shear fractures inside the bridge would not be met in the absence of fluids. This suggests a significant fluid pressure effect inside the bridge. Direct evidence of failure-related fluid flow events can be observed along boundary faults and at the tips of bridge faults. The fault mesh of the compressive bridge consists of pre-existing faults and several new fault generations related to the development of the bridge. Each bridge fault generation shows numerous episodes of reactivation.
5. Finite-element analysis of compressive and extensional bridges along a dextral strike-slip fault, the former analogous to the structures studied at St Donats, showed:
 - (i) For a compressive bridge, the σ_1 orientation within the bridge rotates towards parallelism with the bridge-bounding strike-slip faults during the growth of the overlap zone. This is in accord with the observed rotation of the stress pattern at St Donats that is coeval with bridge development. The modelled mean stress pattern shows a regional maximum within the bridge and two pairs of local maxima/minima situated at the tips of the propagating bridge-bounding strike-slip faults. The local maxima are developed at the advancing side or compressional quadrant and the local minima at the retreating side or extensional quadrant of the strike-slip fault tips. The stress build-up, produced by the convergent relative slip on the two bridge-bounding faults, controls the mean stress concentration within the bridge.
 - (ii) In the case of an extensional bridge, the minimum principal compressive stress σ_3 rotates towards parallelism with the bridge-bounding strike-slip faults during the growth of the overlap zone. The modelled mean stress pattern shows a similar pattern to that of the compressive bridge, with the stress maxima and minima locations interchanged. The stress decrease within the extensional bridge, produced by the divergent relative slip on the two bridge-bounding faults, controls the mean stress minimum within the bridge.
 - (iii) At all stages in bridge development and for both compressive and extensional bridges, the greater the differential stress ($\sigma_1 - \sigma_3$) the more pronounced are the mean stress maxima and minima in the boundary fault tip regions.
 - (iv) During all boundary fault stages of bridge evolution, the mean stress maximum within a compressive bridge centre and the mean stress minimum within an extensional bridge centre are more pronounced with greater differential stress ($\sigma_1 - \sigma_3$).
 - (v) During all boundary fault stages of bridge evolution, the mean stress increase and decrease in compressive and extensional bridges, respectively, is enhanced when the boundary faults have reduced friction.
6. Mean stress maxima form potential pressure gradients to drive fluid flow out of the bridge. Mean stress minima

form potential pressure gradients to suck fluid flow into the bridge. Slip along the boundary fault connecting different bridge types, allows fluid to migrate along the fault during the interval between its failure and the later collapse of its permeability system. The closer adjacent compressive and extensional bridges are along the main strike-slip fault, the greater will be the gradient between their associated mean stress anomalies. The greater the mean stress gradient is, the larger will be the fluid flow rate along the main strike-slip fault.

7. Cyclic mean stress build-ups during the development history of the strike-slip fault bridge provide a long-lasting fluid-driving mechanism. Cyclic fracturing and faulting provides fluid migration pathways.

Acknowledgements

Reviews by Simon A. Kattenhorn, Jonathan S. Caine and Agust Gudmundsson considerably improved the paper. The fracture study was made when MN, RAG, SV and TMH were at Cardiff University. The work of MN was supported by the Royal Society and Alexander von Humboldt Funds. Large amount of tables and figures documenting the field study and numerical modelling in detail is available in the JSG electronic annex.

References

- Angelier, J., 1989. From orientation to magnitudes in paleostress determinations using fault slip data. *Journal of Structural Geology* 11, 37–50.
- Antonellini, M., Mollema, P.N., 2000. A natural analog for a fractured and faulted reservoir in dolomite: Triassic Sella Group, northern Italy. *American Association of Petroleum Geologists Bulletin* 84, 314–344.
- Aydin, A., Nur, A., 1985. The types and role of stepovers in strike-slip tectonics. In: Biddle, K.T., Christie-Blick, N. (Eds.), *Strike-slip Deformation, Basin Formation, and Sedimentation*. Special Publication of the Society of Economic Paleontology and Mineralogy 37, pp. 35–44.
- Barton, C.A., Zoback, M.D., Moos, D., 1995. Fluid flow along potentially active faults in crystalline rock. *Geology* 23, 683–686.
- Batzle, M.L., Simmons, G., 1977. Geothermal systems; rocks, fluids, fractures. In: Heacock, J.G., Keller, G.V., Oliver, J.E., Simmons, G. (Eds.), *The Earth's Crust; its Nature and Physical Properties*. Geophysical Monograph 20, pp. 233–242.
- Booker, J.R., 1974. Time dependent strain following faulting of a porous medium. *Journal of Geophysical Research* 79, 2037–2044.
- Bredehoeft, J.D., Djevanshir, R.D., Belitz, K.R., 1988. Lateral fluid flow in a compacting sand–shale sequence: South Caspian Basin. *American Association of Petroleum Geologists Bulletin* 72, 416–424.
- Byerlee, J.D., 1993. Model for episodic flow of high-pressure water in fault zones before earthquakes. *Geology* 21, 303–306.
- Caine, J.S., 1999. The architecture and permeability structure of brittle fault zones. Ph.D. thesis, University of Utah.
- Caine, J.S., Forster, C.B., 1999. Fault zone architecture and fluid flow; insights from field data and numerical modeling. In: Haneberg, W.C., Mozley, P.S., Moore, J.C., Goodwin, L.B. (Eds.), *Faults and Subsurface Fluid Flow in the Shallow Crust*. Geophysical Monograph 113, pp. 101–127.
- Carlsson, A., Olsson, T., 1979. Hydraulic conductivity and its stress dependence. *Proceedings of the Paris Workshop on Low-Flow, Low-Permeability Measurements in Largely Impermeable Rocks*, pp. 249–259.
- Chester, F.M., Logan, J.M., 1986. Composite planar fabric of gouge from the Punchbowl Fault, California. *Journal of Structural Geology* 9, 621–634.
- Connolly, P.T., Cosgrove, J.W., 1999. Prediction of fracture-induced permeability and fluid flow in the crust using experimental stress data. *American Association of Petroleum Geologists Bulletin* 83, 757–777.
- Davidson, G.R., Bassett, R.L., Hardin, E.L., Thompson, D.L., 1998. Geochemical evidence of preferential flow of water through fractures in unsaturated tuff, Apache Leap, Arizona. *Applied Geochemistry* 13, 185–195.
- Davies, P., Williams, A.T., Bomboe, P., 1991. Numerical modelling of Lower Lias rock failures in the coastal cliffs of South Wales. In: Kraus, N.C., Ginger-ich, K.J., Kriebel, D.J. (Eds.), *Coastal Sediments '91*. American Society of Civil Engineering, New York, pp. 1599–1612.
- Ferrill, D.A., Winterle, J., Wittmeyer, G., Sims, D., Colton, S., Armstrong, A., 1999. Stressed rock strains groundwater at Yucca Mountain, Nevada. *Geologic Society of America Today* 9, 1–8.
- Finkbeiner, T., Barton, C.A., Zoback, M.D., 1997. Relationships among in-situ stress, fractures and faults, and fluid flow: Monterey Formation, Santa Maria Basin, California. *American Association of Petroleum Geologists Bulletin* 81, 1975–1999.
- Fisher, A.T., Zwart, G., Shipley, T., Ogawa, Y., Ashi, J., Blum, P., Brueckmann, W., Filice, F., Goldberg, D., Henry, P., Housen, B., Jurado, M.J., Kastner, M., Labaume, P., Laier, T., Leitch, E., Maltman, A., Meyer, A., Moore, J.C., Moore, G., Peacock, S., Rabaute, A., Steiger, T., Tobin, H., Underwood, M., Xu, Y., Yin, H., Zheng, Y., 1996. Relation between permeability and effective stress along a plate-boundary fault, Barbados accretionary complex. *Geology* 24, 307–310.
- Forster, C.B., Evans, J.P., 1991. Hydrogeology of thrust faults and crystalline thrust sheets: results of combined field and modeling studies. *Geophysical Research Letters* 18, 979–982.
- Freeze, R.A., Cherry, J.A., 1979. *Groundwater*. Prentice-Hall, pp. 1–604.
- Gamond, J.F., 1987. Bridge structures as sense of displacement criteria in brittle fault zones. *Journal of Structural Geology* 9, 609–620.
- Geiser, P., 1974. Cleavage in some sedimentary rocks of the central Valley and Ridge province, Maryland. *Geological Society of America Bulletin* 85, 1399–1412.
- Grindley, G.W., Browne, P.R.L., 1976. Structural and hydrological factors controlling the permeability of some hot-water geothermal fields. *Proceedings of the 2nd United Nations Symposium on Development and Use of Geothermal Resources*, New York, pp. 377–386.
- Hancock, P., 1985. Brittle microtectonics: principles and practice. *Journal of Structural Geology* 7, 437–457.
- Hardcastle, K.C., 1989. Possible paleostress tensor configurations derived from fault-slip data in eastern Vermont and western New Hampshire. *Tectonics* 8, 265–284.
- Hardcastle, K.C., Hills, L.S., 1991. BRUTE3 and SELECT: Quickbasic 4 programs for determination of stress tensor configurations and separation of heterogeneous populations of fault-slip data. *Computers and Geosciences* 17, 23–43.
- Hardebeck, J.L., Hauksson, E., 1999. Role of fluids in faulting inferred from stress field signatures. *Science* 285, 236–239.
- Harp, E.L., Wells, W.G., II, Sarmiento, J.G., 1990. Pore pressure response during failure in soils. *Geological Society of America Bulletin* 102, 428–438.
- Homberg, C., Hu, J.C., Angelier, J., Bergerat, F., Lacombe, O., 1997. Characterization of stress perturbations near major fault zones: insights from 2-D distinct-element numerical modelling and field studies (Jura mountains). *Journal of Structural Geology* 19, 703–718.
- Hubbert, M.K., 1940. The theory of ground-water motion. *Journal of Geology* 48, 785–944.
- Jamison, W.R., 1996. Mechanical models of triangle zone evolution. In: Mackay, P.A., Varsek, J.L., Kubli, T.E., Dechesne, R.G., Newson,

- A.C., Reid, J.P. (Eds.), Triangle Zones and Tectonic Wedges. *Bulletin of Canadian Petroleum Geology* 44, pp. 180–194.
- Jiang, Z., Oliver, N.H.S., Barr, T.D., Power, W.L., Ord, A., 1997. Numerical modeling of fault-controlled fluid flow in the genesis of tin deposits of the Malage ore field, Gejiu mining district, China. *Economic Geology* 92, 228–247.
- Klinger, R.E., Rockwell, T.K., 1989. Flexural-slip folding along the Eastern Elmore Ranch Fault in the Superstition Hills Earthquake sequence of November 1987. *Bulletin of Seismological Society of America* 79, 297–303.
- Knipe, R.J., 1993. The influence of fault zone processes and diagenesis on fluid flow. In: Horbury, A.D., Robinson, A. (Eds.), *Diagenesis and Basin Development*. American Association of Petroleum Geologists Studies in Geology 36, pp. 135–151.
- Knipe, R.J., Agar, S.M., Prior, D.J., 1991. The microstructural evolution of fluid flow paths in semi-lithified sediments from subduction complexes. *Philosophical Transactions of the Royal Society of London* 335, 261–273.
- Krantz, R.L., Scholz, C.H., 1977. Critical dilatant volume of rocks at the onset of tertiary creep. *Journal of Geophysical Research* 82, 4893–4898.
- Kukal, Z., 1989. The rate of geological processes. *Earth Science Reviews* 28, 1–284.
- Lama, R.D., Vutukuri, V.S., 1978. *Handbook on Mechanical Properties of Rocks*. *Transtech Publications*, Bay Village.
- Larsen, P.H., 1988. Relay structures in a Lower Paleozoic basement-involved extension system, east Greenland. *Journal of Structural Geology* 10, 3–8.
- Last, N.C., Harper, T.R., 1990. Response of fractured rock subject to fluid injection, Part 1. Development of a numerical model. *Tectonophysics* 172, 1–31.
- Lee, C.H., Farmer, I., 1993. *Fluid Flow in Discontinuous Rocks*. Chapman and Hall, pp. 1–169.
- Lockner, D.A., Moore, D.E., Reches, Z., 1992. Microcrack interaction leading to shear fracture. 33rd Symposium on Rock Mechanics, pp. 807–816.
- Magara, K., 1976. Water expulsion from elastic sediments during compaction—directions and volumes. *American Association of Petroleum Geologists Bulletin* 60, 543–553.
- Mandl, G., 1988. *Mechanics of Tectonic Faulting. Models and Basic Concepts*. Elsevier, Amsterdam.
- Mann, D.M., Mackenzie, A.S., 1990. Prediction of pore fluid pressures in sedimentary basins. *Marine and Petroleum Geology* 7, 55–65.
- Martel, S.J., Boger, W.A., 1998. Geometry and mechanics of secondary fracturing around small three-dimensional faults in granitic rock. *Journal of Geophysical Research* 103, 21299–21314.
- Martel, S.J., Pollard, D.D., Segall, P., 1988. Development of simple strike-slip fault zones, Mount Abbot quadrangle, Sierra Nevada, California. *Bulletin of the Geological Society of America* 100, 1451–1465.
- Miller, S.A., Nur, A., Olgaard, D.L., 1996. Earthquakes as a coupled shear stress–high pore pressure dynamical system. *Geophysical Research Letters* 23, 197–200.
- Mollema, P.N., Antonellini, M.A., 1996. Compaction bands: a structural analog for anti-mode I cracks in aeolian sandstone. *Tectonophysics* 267, 209–228.
- Moore, J.C., Orange, D., Stiles, S., Geddes, D., 1990. Fluid and hydrocarbon migration at active margins; a conceptual synthesis of results from the Barbados Ridge and Pacific Northwest. *AAPG Bulletin* 74, 724–725.
- Nemčok, M., Gayer, R.A., 1996. Modelling palaeostress magnitude and age in extensional basins: a case study from the Mesozoic Bristol Channel Basin, UK. *Journal of Structural Geology* 18, 1301–1314.
- Nemčok, M., Gayer, R.A., Miliorizos, M., 1995. Structural analysis of the inverted Bristol Channel Basin: implications for the geometry and timing of the fracture porosity. In: Buchanan, J.G., Buchanan, P.G. (Eds.), *Basin Inversion*. Geological Society Special Publication 82, pp. 355–392.
- Nur, A., Booker, J.R., 1972. Aftershocks caused by pore fluid flow. *Science* 175, 885.
- Ohlmacher, G.C., Aydin, A., 1997. Mechanics of vein, fault and solution surface formation in the Appalachian Valley and Ridge, northeastern Tennessee, USA: implications for fault friction, state of stress and fluid pressure. *Journal of Structural Geology* 19, 927–944.
- Oliver, J., 1986. Fluids expelled tectonically from orogenic belts. *Geology* 14, 99–102.
- Parry, W.T., Bruhn, R.L., 1986. Pore fluid and seismogenic characteristics of fault rock at depth on the Wasatch Fault, Utah. *Journal of Geophysical Research* 91, 730–744.
- Parry, W.T., Bruhn, R.L., 1990. Fluid pressure transients on seismogenic normal faults. *Tectonophysics* 179, 335–344.
- Peacock, D.C.P., Sanderson, D.J., 1995. Strike-slip relay ramps. *Journal of Structural Geology* 17, 1351–1360.
- Petit, J.P., 1987. Criteria for the sense of movement on fault surfaces in brittle rocks. *Journal of Structural Geology* 9, 597–608.
- Philip, H., Rogozhin, E., Cisternas, A., Bosquet, J.C., Borisov, B., Karakhanian, A., 1992. The Armenian Earthquake of 1988 December 7: faulting and folding, neotectonics and palaeoseismicity. *Geophysical Journal International* 110, 141–158.
- Ramsay, J.G., Huber, M.I., 1987. *The Techniques of Modern Structural Geology*. Academic Press, London.
- Roberts, S., Nunn, J.A., Cathles, L., Cipriani, F.D., 1996. Expulsion of abnormally pressured fluids along faults. *Journal of Geophysical Research* 101, 28231–28252.
- Rockwell, T.K., Keller, E.A., Dembroff, G.R., 1988. Quaternary rate of folding of the Ventura anticline, western Transverse Ranges, southern California. *American Geological Society Bulletin* 100, 850–858.
- Scholz, C.H., 1968. Microfracturing and the inelastic deformation of rock in compression. *Journal of Geophysical Research* 73, 1417–1432.
- Scholz, C.H., 1990. *The Mechanics of Earthquakes and Faulting*. Cambridge University Press, Cambridge.
- Screaton, E.J., Wuthrich, D.R., Dreiss, S.J., 1990. Permeabilities, fluid pressures and flow rates in the Barbados Ridge Complex. *Journal of Geophysical Research* 95, 8997–9008.
- Segall, P., Pollard, D.D., 1980. Mechanics of discontinuous faults. *Journal of Geophysical Research* 85, 4337–4350.
- Shi, Y., Wang, C.Y., 1986. Pore pressure generation in sedimentary basins: overloading versus aquathermal. *Journal of Geophysical Research* 91, 2153–2162.
- Sibson, R.H., 1985. Stopping of earthquake ruptures at dilational fault jogs. *Nature* 316, 248–251.
- Sibson, R.H., 1989. Earthquake faulting as a structural process. *Journal of Structural Geology* 11, 1–14.
- Sibson, R.H., 1990. Conditions for fault-valve behaviour. In: Knipe, R.J., Rutter, E.H. (Eds.), *Deformation Mechanisms, Rheology and Tectonics*. Geological Society Special Publication 54, pp. 15–28.
- Sibson, R.H., 1994. Crustal stress, faulting, and fluid flow. In: Parnell, J. (Ed.), *Geofluids: Origin, Migration and Evolution of Fluids in Sedimentary Basins*. Geological Society Special Publication 78, pp. 69–84.
- Smith, L., Forster, C.B., Evans, J.P., 1990. Interaction between fault zones, fluid flow, and heat transfer at the basin scale. In: Newman, S.P., Neretnieks, I. (Eds.), *International Association of Hydrologic Sciences; Selected Papers in Hydrology* 2, 41–67.
- Smith, R., Wiltschko, D.V., 1996. Generation and maintenance of abnormal fluid pressures beneath a ramping thrust sheet: isotropic permeability experiments. *Journal of Structural Geology* 18, 951–970.
- Sylvester, A.G., 1988. Strike-slip faults. *Geological Society of America Bulletin* 100, 1666–1703.
- Treiman, J.E., 1995. Surface faulting near Santa Clarita. *California Division of Mines and Geology, Special Publication* 116, 103–110.
- Tsang, C.F., 1999. Linking thermal, hydrological, and mechanical processes in fractured rocks. *Annual Review of Earth and Planetary Sciences* 27, 359–384.
- Walsh, J.B., 1981. Effect of pore pressure and confining pressure on

- fracture permeability. *International Journal of Rock Mechanics and Mining Sciences* 18, 429–435.
- Waters, R.A., Lawrence, D.J.D., Ivimey-Cook, H.C., Mitchell, M., Warrington, G., White, D.E., Lewis, M.A., 1987. Geology of the South Wales Coalfield, Part II, the country around Cardiff. Memoir for 1:50,000 geological sheet 263 (England and Wales), Third edition, Memoirs of the British Geologic Survey, pp. 1–114.
- Willemse, E.J.M., Peacock, D.C.P., Aydin, A., 1997. Nucleation and growth of strike-slip faults in limestones from Somerset, UK. *Journal of Structural Geology* 19, 1461–1477.
- Wojtal, S., Mitra, G., 1986. Strain hardening and strain softening in fault zones from foreland thrusts. *Geological Society of America Bulletin* 97, 674–687.
- Yielding, G., Jackson, J.A., King, G.C.P., Sinval, H., Vita-Finzi, C., Wood, R.M., 1981. Relations between surface deformation, fault geometry, seismicity and rupture characteristics during the El Asnam (Algeria) earthquake of 10 October, 1980. *Earth and Planetary Science Letters* 56, 287–304.